Current-Sensorless Robust Sliding Mode Control for the Interleaved DC-DC Boost Converter

Said Oucheriah (soucheria@niu.edu).
Department of Engineering Technology Northern Illinois University, Illinois, USA.
.

***Abstract*—A current-sensorless, PWM-based robust sliding mode control strategy for the interleaved DC-DC boost converter is proposed that eliminates the need for leg or input current sensors and requires only output-voltage measurement. The proposed extended state estimator maps the multi-phase converter to a mono-phase equivalent, successfully absorbing structural phase asymmetries and parasitic variations into a single lumped uncertainty term. This observer simultaneously estimates the derivative of the output voltage alongside the composite lumped uncertainty, which includes inductor parasitic resistances, parameter variations, input voltage and load changes. A systematic parameter-tuning procedure based on estimator pole placement and open-loop bandwidth guidelines guarantees a critically damped dominant estimation response. Comprehensive multi-case simulations validate the closed-loop system under parametric uncertainties and parasitics, severe unbalanced operating conditions of the two phases, load resistance and input voltage changes and high-frequency noise injection.**

Keywords: Robust sliding mode control, interleaved DC-DC boost converter, current-sensorless control, extended state estimator.

I. Introduction

DC-DC converters are subjected to external disturbances, parameter uncertainties, and parasitics that must be taken into account in the design of robust controllers to tightly track the output reference voltage and seek a reduction in the number of sensors needed for their implementation. PWM-sliding mode control (SMC) in conjunction with disturbance estimators is a powerful nonlinear control strategy that can be used. However, in many cases, the designed controllers require knowledge of the inductor current. Its measurement can present challenges in the presence of external disturbances and high-frequency noise that can be amplified, leading to chattering in the control signal. This has led to the use of current sensor-free controllers, which offer a reduction in cost and an improvement in the reliability and miniaturization of the device.

In the context of DC-DC boost converters [1-7], the design of robust current sensor-free controllers is a challenging task since the boost converter is a nonminimum phase system. While many of these approaches effectively address the issue of output voltage regulation of DC-DC boost converters, they often have limitations. Some control laws proposed are complicated and computationally intensive to render them impractical in real applications. They may also involve many design parameters that require very laborious parameter tuning, with some lacking rigorous stability analysis of the closed-loop systems. Lastly, with few exceptions, robustness tests to parameter uncertainties and parasitics of the converter are not analyzed and ignored in simulations and may lead to substantial steady-state errors in the output response. To address these problems, an extended state estimator was previously developed by the author in [8] for the single-phase topology. This paper expands upon that foundational framework to solve the unique challenges of multi-phase configurations.

Recently, there is a great interest in interleaved boost converter (IBC) topology, which is being rapidly adopted in renewable energy systems, electric vehicles, and battery charging systems. They are characterized by multiple parallel-connected boost converter stages and offer many advantages over the classical boost converter. These are a reduction in thermal and electrical component stress due to current-sharing capability, an increase in efficiency and power handling capability and a reduction in passive component sizes as compared to the traditional single phase converter.

In [9], a nonlinear disturbance observer (NDO)-based sliding-mode control algorithm is proposed to estimate two lumped disturbances whose derivatives in the limit are assumed zero. The implementation requires the output voltage, the input current and input voltage measurements. In [10], a super-twisting sliding mode control law is proposed for interleaved dc-dc boost converter for fuel cell application based on the double-loop control structure containing two inductor current inner-loops and an output voltage outer-loop. An extended-state-observer (ESO) is used to estimate the total disturbance that comprises the unknown load power and parametric variations. The implementation of the controller requires an inductor current sensor for each phase and the measurements of the input and output voltages. In [11], a robust model predictive control is proposed to regulate the output voltage of a DC-DC floating interleaved boost converter (FIBC) in the presence of parametric uncertainties. The controller is also able to handle input-output constraints. The proposed control algorithm requires extensive computations solving online min-max optimization problems which makes it of little practical interest and unsuitable for systems with low processing capabilities. Also, it needs a sensor to measure the inductor current.

The study in [12] considers an interleaved DC/DC boost converter supplying a DC-bus with generally unknown loads connected to it. An observer based adaptive controller using the immersion and invariance observer with an energy shaping plus damping injection passivity based controller is proposed.

However, the controller requires the measurement of each leg inductor current to ensure equal leg currents. In [13], a controller that is composed of an inner voltage PI loop and an outer voltage PI loop is proposed for the interleaved boost converter. The implementation of the controller requires one input current sensor and one voltage sensor.

In [14] and [17] a robust sliding mode nonlinear controller is designed for an interleaved boost converter based on an extended linearization and active compensation of the lumped disturbance estimated by a linear extended state observer. Simulation and experimental results show that the proposed controller is robust against parameter uncertainties and external disturbances. However, an input current sensor is required for the implementation of the controller.

In [15], a nonlinear fast terminal sliding mode control and a state and disturbance estimation algorithm to estimate the inductor current and a lumped disturbance that includes the load resistance for a two-phase interleaved boost converter is proposed. The stability of the observer is analyzed using Kharitonovs stability criteria. However, the implementation of the controller requires the measurement of the input voltage. In [16], an integral sliding mode controller for the control of a 2PIBC converter is proposed. A lumped disturbance that comprises parameter uncertainties, input voltage and load resistance is estimated using a disturbance observer. The implementation of the controller requires the measurement of the input current.

To address these limitations, this paper proposes a novel current-sensorless robust controller. The main contributions are summarized as follows:

1) Single-Sensor Implementation: The proposed control implementation requires only the measurement of the output voltage, completely eliminating the need for input or leg current sensors in an interleaved configuration.

2) Asymmetry-Compensated State Estimator: A unique mathematical mapping reduces the multi-phase plant to an equivalent mono-phase structure without assuming matched leg parameters. Consequently, any physical phase asymmetries ($L_1 \neq L_2, R_{L1} \neq R_{L2}$), circuit imbalances, and structural non-idealities are explicitly captured and actively compensated for by a single lumped uncertainty estimator.

3) Deterministic Parameter Tuning: An analytical, step-by-step gain selection methodology is established based on open-loop bandwidth boundaries, eliminating empirical trial-and-error while mathematically guaranteeing a critically damped estimation response.

4) Robustness Evaluation under Non-Ideal Conditions: The robustness, chattering suppression, and dynamic regulation capabilities of the closed-loop system are thoroughly verified under severe non-ideal operations, including parameter mismatches, high-frequency noise, and time-varying loads.

The remainder of this paper is organized as follows. Section II details the mathematical modeling, the detailed design of the extended state estimator, the sliding mode controller synthesis, and the closed-loop stability analysis. Section III presents the multi-case simulation validation results under noise and parameter uncertainties. Finally, Section IV concludes the paper.

II. Robust sliding mode control design

A. Two-phase interleaved boost converter averaged model

A basic two-phase interleaved boost converter averaged model is shown in Figure 1. Under continuous conduction

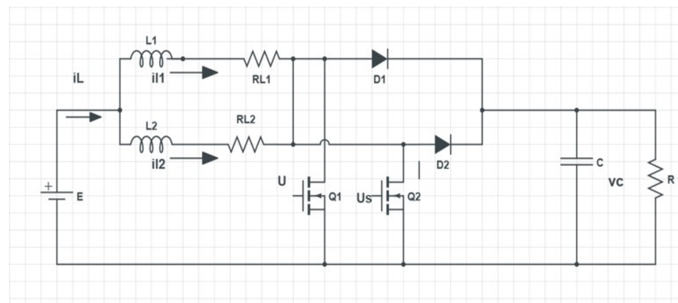

Fig. 1. Circuit diagram of the two-phase interleaved boost converter.

mode, the averaged model is:

$$\begin{aligned}
\dot{i}_{L_1} &= -\frac{R_{L_1}}{L_1} i_{L_1} - (1-u)\frac{v_c}{L_1} + \frac{E}{L_1} \\
\dot{i}_{L_2} &= -\frac{R_{L_2}}{L_2} i_{L_2} - (1-u)\frac{v_c}{L_2} + \frac{E}{L_2} \\
\dot{v}_c &= (1-u)\frac{i_{L_1}}{C} + (1-u)\frac{i_{L_2}}{C} - \frac{v_c}{RC}
\end{aligned} \tag{1}$$

where i_{L_1} and i_{L_2} represent the average inductor currents through inductors L_1 and L_2, respectively, v_c is the output voltage across the capacitor C. The unknown parameters E and R represent the input voltage and the load resistance, respectively. However, their respective nominal values E_o and R_o are assumed known for the implementation of the controller. The control input u to the converter is the duty ratio function and u_s is the same duty ratio as u but staggered in phase by an angle of 180^o.

System (1) can be written as:

$$\begin{aligned}
\dot{i}_{L_1} &= -(1-u)\frac{v_c}{L_o} + \frac{E_o}{L_o} + d_1 \\
\dot{i}_{L_2} &= -(1-u)\frac{v_c}{L_o} + \frac{E_o}{L_o} + d_2 \\
\dot{v}_c &= (1-u)\frac{i_{L_1}}{C_o} + (1-u)\frac{i_{L_2}}{C_o} + d_3
\end{aligned} \tag{2}$$

where L_o and C_o are nominal values.

$$\begin{aligned}
d_1 &= -\frac{R_{L_1}}{L_1} i_{L_1} + (1-u)\left[\frac{1}{L_o} - \frac{1}{L_1}\right] v_c + \frac{E}{L_1} - \frac{E_o}{L_o} \\
d_2 &= -\frac{R_{L_2}}{L_2} i_{L_2} + (1-u)\left[\frac{1}{L_o} - \frac{1}{L_2}\right] v_c + \frac{E}{L_2} - \frac{E_o}{L_o} \\
d_3 &= (1-u)\left[\frac{1}{C} - \frac{1}{C_o}\right] i_{L_1} + (1-u)\left[\frac{1}{C} - \frac{1}{C_o}\right] i_{L_2} - \frac{v_c}{RC}
\end{aligned} \tag{3}$$

This yields the equivalent mono-phase boost converter model described by the following equations:

$$\begin{aligned}
\dot{i}_L &= -2(1-u)\frac{v_c}{L_o} + \frac{2E_o}{L_o} + d_4 \\
\dot{v}_c &= (1-u)\frac{i_L}{C_o} + d_3
\end{aligned} \tag{4}$$

where $i_L = i_{L_1} + i_{L_2}, d_4 = d_1 + d_2$ and E_o, L_o and C_o are the known nominal values of the input voltage E, the leg inductances L_{1o} =$\mathrm{L}_{2o} = L_o$, and the capacitor C, respectively. In addition to the inductor parasitics, other parasitics such as the MOSFET on-resistance, the diode forward resistance, the conducting voltage of the diode and the capacitor equivalent series resistance could have easily been lumped in the disturbance signal $d(t)$.
It is worth noting that the formulated lumped disturbance d_4 directly encapsulates the structural variations, parasitic deviations, and parameter mismatches between the interleaved legs. By mapping these asymmetries into a unified disturbance term, the requirement for identical phase dynamics ($L_1 = L_2$ and $R_{L1} = R_{L2}$) is entirely eliminated, allowing the controller to maintain robust regulation despite severe physical imbalances.

Taking the derivative of both sides of the second equation of (4) and using the expression for $\dot{i}_L$ given by the first equation of (4) yields

$$\ddot{v}_c = \frac{u}{L_o C_o}[4v_c - 2E_o] + d \tag{5}$$

where

$$d = -\frac{2v_c}{L_o C_o}(1+u^2) + \frac{2E_o}{L_o C_o} + \frac{(1-u)}{C_o}d_4 + \dot{d}_3 - \dot{u}\frac{i_L}{C_o} \tag{6}$$

Let

$$\begin{aligned} e_2 &= v_c - V_{ref} \\ e_1 &= \dot{e}_2 \end{aligned} \tag{7}$$

Using the substitution $v_c = e_2 + V_{ref}$ and $\ddot{v}_c = \dot{e}_1$ into (5) yields

$$\begin{aligned} \dot{e}_1 &= \frac{u}{L_o C_o}\Big[4(e_2 + V_{ref}) - 2E_o\Big] + d \\ \dot{e}_2 &= e_1 \end{aligned} \tag{8}$$

B. Design of the extended state estimator

By using the lumped uncertainty d given by (6) as a state variable, the extended state estimator for the system (8) is

$$\begin{aligned} \dot{q}_1 &= \frac{u}{L_o C_o}\Big[4(e_2 + V_{ref}) - 2E_o\Big] \\ &\quad + q_3 + K_3 e_2 - K_1 q_1 - K_1^2 e_2 \\ \dot{q}_2 &= q_1 + K_1 e_2 + K_2 \tilde{q}_2 \\ \dot{q}_3 &= -K_3 q_1 - K_1 K_3 e_2 \end{aligned} \tag{9}$$

The states $\hat{e}_1,\ \hat{e}_2$ and $\hat{d}$ are the estimates of e_1, e_2 and d respectively and are given by:

$$\hat{e}_1 = q_1 + K_1 e_2,\ \hat{e}_2 = q_2,\ \hat{d} = q_3 + K_3 e_2 \tag{10}$$

with $\tilde{q}_2 = e_2 - \hat{e}_2$. The parameters K_1, K_2 and K_3 are the estimator gains. Using (8), (9) and (10), the dynamics of the state errors are

$$\begin{aligned} \dot{\tilde{e}}_1 &= -K_1 \tilde{e}_1 + \tilde{d} \\ \dot{\tilde{e}}_2 &= \tilde{e}_1 - K_2 \tilde{e}_2 \\ \dot{\tilde{d}} &= -K_3 \tilde{e}_1 + \dot{d} \end{aligned} \tag{11}$$

with $\tilde{e}_1 = e_1 - \hat{e}_1,\ \tilde{e}_2 = e_2 - \hat{e}_2$ and $\tilde{d} = d - \hat{d}$. System (11) can be written in compact form as

$$\dot{\tilde{e}} = A\tilde{e} + B\dot{d} \tag{12}$$

where $\tilde{e} = [\tilde{e}_1,\ \tilde{e}_2,\ \tilde{d}]^T$ and

$$A = \begin{bmatrix} -K_1 & 0 & 1 \\ 1 & -K_2 & 0 \\ -K_3 & 0 & 0 \end{bmatrix},\ B = \begin{bmatrix} 0 \\ 0 \\ 1 \end{bmatrix} \tag{13}$$

Assumption 1: We assume that for any bounded time-varying lumped disturbance d we have

$$\delta = \sup_{t \in [0\ \infty)} \|\dot{d}\| < \infty \tag{14}$$

This assumption applies to the averaged model where it is reasonable to assume that the states and parameter uncertainties are bounded and sufficiently smooth. For the switched model, the controller uses the estimated disturbance rather than the instantaneous switching-ripple-contaminated one. The estimator behaves like a low-pass observer: it tracks the average or low-frequency component of the lumped disturbance and rejects much of the high-frequency switching ripple. Therefore, accurate point-by-point estimation of the switched signal is not required for good voltage regulation.

The eigenvalues of the system matrix A are determined from the characteristic equation

$$\begin{aligned} s^3 + (K_1 + K_2)\, s^2 + \big(K_1 K_2 + K_3\big)\, s \\ + K_2 K_3 = 0 \end{aligned} \tag{15}$$

Remark 1: For any $K_1 > 0, K_2 > 0$ and $K_3 > 0$, the poles are on the left-half side of the complex plane with the matrix A being Hurwitz. The extended state estimator's dynamic response depends entirely on the choice of the tuning gains. To ensure a critically damped dominant estimation response without any unwanted oscillation, the estimator gains are selected as

$$K_3 = \frac{K_1^2}{4},\ K_2 = 5\sqrt{K_3} \tag{16}$$

In this case, the estimation error dynamics feature two identical real dominant poles at $-K_1/2$ and a third non-dominant pole at $-5K_1/2$, which sits exactly five times further to the left in the complex plane. The state errors are strictly and tightly bounded by

$$\begin{aligned} \limsup_{t\to\infty} |\tilde{e}_1(t)| \le \frac{\delta}{K_3},\ \limsup_{t\to\infty} |\tilde{e}_2(t)| \le \frac{\delta}{K_2 K_3} \\ \limsup_{t\to\infty} |\tilde{d}(t)| \le \frac{\delta K_1}{K_3} \end{aligned} \tag{17}$$

Remark 2: If $\lim_{t\to\infty} \dot{d}(t) = 0$, then all states will asymptotically decay to zero as time goes to infinity and we have

$$\lim_{t\to\infty} \tilde{e}_1 = 0,\ \lim_{t\to\infty} \tilde{e}_2 = 0,\ \lim_{t\to\infty} \tilde{d} = 0 \tag{18}$$

Since K_3 is typically a very high gain, the ultimate estimator-error bounds are usually small and approach uniformly 0 in $t \in [0\ \infty)$ as $K_3 \to \infty$.

C. Design of the controller and stability analysis

We consider the following sliding surface

$$\sigma = \hat{e}_1 + \gamma\hat{e}_2 - K_1 e_2 = q_1 + \gamma q_2 \tag{19}$$

where we have used $\hat{e}_1 = q_1 + K_1 e_2$ and $q_2 = \hat{e}_2$ and $\gamma > 0$ is a design parameter. We consider the following controller:

$$\begin{aligned} u &= \alpha\left(K_1 - \gamma\right) q_1 - \alpha q_3 \\ &+ \alpha\left(-K_3 + K_1^2 - \gamma K_1\right) e_2 - \alpha K_2 \gamma \tilde{q}_2 - \alpha K_4 \sigma \end{aligned} \tag{20}$$

where

$$\alpha = \frac{L_o C_o}{[4(e_2 + V_{ref}) - 2E_o]} \tag{21}$$

Using (19), the controller (20) is derived by differentiating σ with respect to time and setting $\dot{\sigma} = 0$. The last term $\alpha K_4 \sigma$ is added for manifold-restoring action as explained below in the sequel.

The substitution of the controller u into the derivative of (19) leads to

$$\dot{\sigma} = -K_4 \sigma \tag{22}$$

and therefore we have $\dot{\sigma}\sigma = -K_4\sigma^2 < 0$ which ensures the sliding mode condition. Equation (22) admits as a solution

$$\sigma(t) = \sigma(0)e^{-K_4 t} \tag{23}$$

Using the initial conditions $q_1(0) = 0,\ q_2(0) = 0$ for the extended state estimator (9), yields $\sigma(0) = 0$ and in this case $\sigma(t) = 0$ for all $t \geq 0$. Hence, the closed-loop trajectory begins on the sliding manifold and remains invariant on it, eliminating the reaching phase.
Although the ideal averaged model remains exactly on the manifold when $\sigma(0) = 0$, a positive K_4 is still needed for the switched model. Reference changes accompanied by PWM effects, duty-ratio saturation, and measurement noise can temporarily cause $\sigma(t_d) \neq 0$ where t_d is the onset of a disturbance or a reference change. In this case we have

$$\sigma(t) = \sigma(t_d)e^{-K_4(t-t_d)},\ t \geq t_d \tag{24}$$

The gain K_4 provides manifold-restoring action. For the choice of the gain K_4, there is a trade-off between a large value for a fast recovery with possible aggressive duty ration behavior, or a small value to smooth the transient control effort and prevent aggressive chattering during sudden voltage reference steps.

Assumption 2: Upon powering up the boost converter and before the activation of the controller, the output voltage naturally satisfies $v_c(t) \geq E_o - V_D > \frac{E_o}{2}$ where V_D is the forward voltage drop of the diodes. This initial voltage is established via passive pre-charging as current flows from the input voltage directly through the inductor and the boost diode. Consequently, the denominator term $(4v_c - 2E_o)$ in (21) is strictly bounded away from zero, eliminating the mathematical singularity in the parameter α. Furthermore, it is assumed that external system disturbances remain sufficiently small such that the resulting control effort in (20) satisfies the physical constraints $0 < u(t) < 1$ without hitting saturation limits.

Theorem 1: Consider system (1), the extended state estimator (9), and controller (20). Suppose Assumptions 1 and 2 hold and $\gamma > K_1$. Then the output-voltage tracking error is globally uniformly ultimately bounded to a ball $\Omega(r)$ centered at V_{ref} with a radius r

$$r = \frac{1}{(\gamma - K_1)}\left[\frac{\delta}{K_3}\left(1 + \frac{\gamma}{K_2}\right)\right] \tag{25}$$

with a decay rate $(\gamma - K_1)$.

Proof: Substituting $(e_1 - \tilde{e}_1)$ for $\hat{e}_1$, $(e_2 - \tilde{e}_2)$ for $\hat{e}_2$ in equation (19) and solving for e_1 yields

$$e_1 = -(\gamma - K_1)e_2 + \tilde{e}_1 + \gamma\tilde{e}_2 + \sigma \tag{26}$$

Using $e_1 = \dot{v}_c$ and $e_2 = v_c - V_{ref}$ into (26) yields the following dynamic equation

$$\dot{v}_c(t) + (\gamma - K_1)(v_c(t) - V_{\text{ref}}) = \tilde{e}_1(t) + \gamma\tilde{e}_2(t) + \sigma \tag{27}$$

Applying the integration factor $e^{-(\gamma-K_1)t}$ and invoking the triangle inequality yields:

$$\begin{aligned} |v_c(t) - V_{\text{ref}}| \leq |e_2(0)|e^{-(\gamma-K_1)t} + \textstyle\int_0^t e^{-(\gamma-K_1)(t-\tau)}[|\tilde{e}_1(\tau)| \\ +\gamma|\tilde{e}_2(\tau)| + |\sigma(\tau)|]d\tau. \end{aligned} \tag{28}$$

Since $\limsup_{t\to\infty} |\sigma(t)| = 0$, substitution of (17) gives

$$\limsup_{t\to\infty} |v_c(t) - V_{\text{ref}}| \leq \frac{1}{\gamma - K_1}\left[\frac{\delta}{K_3}\left(1 + \frac{\gamma}{K_2}\right)\right] = r. \tag{29}$$

and consequently, v_c is uniformly convergent to a ball centered at V_{ref} with a radius r given by (25) and a decay rate $(\gamma - K_1)$.

D. Boundedness of the Line Current

For each phase j = 1, 2, the physical inductor-current equation is

$$\dot{i}_{L_j} = -\frac{R_{L_j}}{L_j} i_{L_j} - (1-u)\frac{v_c}{L_j} + \frac{E}{L_j} \tag{30}$$

Under Assumption 2, the implemented duty ratio satisfies $0 < u < 1,\ t \geq 0$ and is therefore bounded. Furthermore, Theorem 1 establishes that the output voltage $v_c(t)$ is bounded. Assuming that the input voltage E(t) is bounded then we can define

$$F_j = sup_{t\geq 0}|E(t) - (1 - u(t))v_c(t)| \tag{31}$$

and we have

$$|i_{L_j}| \leq |i_{L_j}(0)|e^{-\frac{R_{L_j}}{L_j}t} + \frac{F_j}{R_{L_j}}\left[1 - e^{-\frac{R_{L_j}}{L_j}t}\right] \tag{32}$$

Therefore,

$$|i_{L_j}| \leq max(|i_{L_j}(0)|, \frac{F_j}{R_{L_j}} \tag{33}$$

and since $i_L = i_{L_1} + i_{L_2}$ it follows:

$$|i_L| \leq max\left(|i_{L_1}(0)|, \frac{F_1}{R_{L_1}}\right) + max\left(|i_{L_2}(0)|, \frac{F_2}{R_{L_2}}\right) \tag{34}$$

and the line current is bounded.

Remark 3: Let the $\tau_o = R_o C_o$ be the nominal time constant of the open-loop system with a decay constant $a_o = \tau_o^{-1}$. In view of (9), (17) and (24), a possible general guideline for the choice of the controller and estimator gains is:
1) Choose $K_1 = m a_o$, with $N_1 \leq m \leq N_2$.
2) Choose $\gamma = 1.25 K_1$.
3) Choose $K_3 = \frac{K_1^2}{4}$ to ensure a critically damped dominant subsystem with two identical real dominant poles at $-K_1/2$.
4) Choose $K_2 = 5\sqrt{K_3}$ to ensure that the third non-dominant pole is at $-5K_1/2$, which sits exactly five times further to the left in the complex plane.
5) If the performance is not adequate, increase m in step 1 and repeat.
To determine N_1 and N_2, the control loop crossover and estimator bandwidth must be kept well below the Nyquist frequency of $f_s/2$, where f_s is the switching frequency. As a general rule we use the non dominant $5K_1/2$ pole which is the highest frequency dynamic tracked by the estimator to be $f_s/10$ and this gives us

$$\frac{5K_1}{2} = \frac{5 a_o m}{2} \leq \frac{2\pi f_s}{10} \implies m \leq N_2 \leq \frac{\pi f_s}{12.5\ a_o} \tag{35}$$

As a conservative baseline we can start at $N_1 = 5$.
To make the dominant estimator dynamics faster than the nominal voltage-error dynamics, choose

$$\gamma - K_1 = \frac{K_1}{4} \implies \gamma = 1.25\ K_1 \tag{36}$$

This selection makes the dominant estimator poles twice as fast as the nominal voltage-error pole, providing a bandwidth-separation factor of two.

For the choice of the gain K_4, there is a trade-off between a large value for fast manifold recovery rate and aggressive duty-ratio behavior, or a small value to smooth the transient control effort and prevent aggressive chattering during sudden voltage reference steps but slower manifold recovery rate.

III. Simulation Results

A. Case 1: Performance analysis of the proposed estimator.

The extended state estimator is tested using the averaged model and the switched model of the IBC. The switching frequency for the sampled model is f_s= 100 kHz. Using the uncertain parameters of Table 1 and Remark 3, as a general guideline, yield $N_2 = 100$ with a baseline $N_1 = 5$. Please note that the only parameters known to the controller for its implementation are the nominal input voltage, the nominal leg inductors, the nominal capacitor and the nominal load resistance listed in Table 1. For a choice of $m = 30$ the gains of the estimator/controller parameters are:

$$K_1 = 7.5\times10^3,\ \gamma = 9.375\times10^3,\ K_2 = 18.750\times10^3, \\ K_3 = 14.0625\times10^6,\ K_4 = 10^3 \tag{37}$$

The initial conditions of the state extended estimator are $q_1(0) = 0,\ q_2(0) = 0$ and $q_3(0) = 0$.

The nominal specifications, asymmetric physical parameters of the interleaved legs, and the calculated controller/estimator gains are summarized in Table 1.

TABLE I
System Specifications and Asymmetric Parameters

Parameter Description	Symbol	Value (Nominal / Actual)
Input Voltage	E	50 V / 60 V
Reference Output Voltage	V_{ref}	100 V / 100 V
Nominal Capacitor	C	200 μF/140 μF
Nominal Load Resistance	R	20 Ω / 26 Ω
Switching Frequency	f_s	100 kHz / 100 kHz
Phase Leg 1 Parameters		
Phase 1 Inductance	L_1	76 μH / 114 μH
Phase 1 Resistance	R_{L1}	0.1 Ω / 0.20 Ω
Phase Leg 2 Parameters		
Phase 2 Inductance	L_2	76 μH / 117 μH
Phase 2 Resistance	R_{L2}	0.1 Ω / 0.30 Ω
Controller & Estimator Gains		
Estimator Gain	K_1	[7.5×10^3]
Estimator Gain	K_2	[18.750×10^3]
Estimator Gain	K_3	[14.0625×10^6]
Sliding Control Gain	K_4	[10^3]
Sliding Surface Design Parameter	γ	[9.375×10^3]

Using the averaged model, Fig.2(a) shows the damped output response $v_c(t)$ reaching the reference voltage V_{ref} with zero steady-error. Figure 2(b) shows the perfect estimation of the lumped uncertainty with zero-steady tracking error. The steady-state of the estimate is $\hat{d} \simeq 8.05\times10^9$.

Using the switched model, Fig. 3(a) shows a similar damped output response as the averaged model case with zero steady-state error. Figure 3(b), depicts the lumped disturbance d and its estimate $\hat{d}$. In this case, there is a substantial steady-state error between d and its estimate $\hat{d}$. This is due to the fact that the switched model introduces inevitable high-frequency switching pulses. Despite the estimation error, the estimator still yields the same steady-state estimate $\hat{d} \simeq 8.05\times10^9$ used in the implementation of the controller. This is a validation of the estimator noise-rejection capability. The estimator successfully rejects the high-frequency switching ripple while maintaining tight tracking of the true average disturbance baseline.

B. Case 2: Robustness to Step Load and Input Voltage Changes under Severe Phase Asymmetry

To evaluate the controller's capability to handle acute parameter imbalances alongside external line and load disturbances, the interleaved boost converter is subjected to severe hardware asymmetries as detailed in Table I. Crucially, the phase parameters are heavily mismatched ($L_1 = 114\,\mu$H vs. $L_2 = 117\,\mu$H, and $RL_1 = 0.2\,\Omega$ vs. $RL_2 = 0.3\,\Omega$), establishing a highly unbalanced baseline operation. At time $t = 0.2$ s, a step load resistance change of $-10\,\Omega$ is applied, followed by a $+10\,\Omega$ step recovery at $t = 0.4$ s. Furthermore, line voltage step disturbances of -5 V and $+5$ V are injected at $t = 0.6$ s and $t = 0.8$ s, respectively.

The simulation is carried out utilizing the sampled switch model operating at a switching frequency $f_s = 100$ kHz. Fig. 4(a) illustrates the time-domain performance of the output voltage $v_c(t)$. Despite the simultaneous presence of severe structural asymmetries and step and input voltage changes, the output voltage tightly tracks the reference voltage with zero steady-state error, negligible settling time, and zero overshoot. The proposed controller is not intended to enforce equal phase-current sharing. Under balanced component conditions, the interleaved topology naturally promotes approximately equal current sharing. Under parameter asymmetry, an unequal current distribution may occur, as illustrated in Fig. 4. Nevertheless, both phases continue to contribute to the total input current, and the proposed sensorless controller maintains accurate output-voltage regulation without individual phase-current measurements or an additional current-balancing loop. The proposed extended state estimator seamlessly captures the asymmetric current divergence within the single lumped uncertainty state $d(t)$. Despite this imbalance, interleaving cancellation still functions effectively: individual phase ripple is 2.08 A, while the total combined input ripple drops significantly to just 0.640 A.

C. Case 3: Robustness to time-varying load resistance with noise, the uncertain parameters of Table 1 and parasitics given in (38).

To assess the robustness of the proposed controller against the noise-contaminated measurements of the output voltage, a band-limited white noise with a noise power of 6.25×10^{-8} V^2/Hz and a sampling time of $1\mu s$ is added to the output voltage to produce a 250 mV_{RMS} (0.0625 V^2 variance). To align with the overall system simulation step size of 1 μs, the block noise sample time is set to 1 μs. Assuming a standard 3σ statistical bound, this corresponds to a practical peak-to-peak noise voltage of 1.5 $\text{V}_{\text{p-p}}$ on the 100 V DC output rail. In addition to the noise, we assume that the converter is subjected simultaneously to the uncertain parameters listed in Table 1, to the parasitics given in (37) and to the time-varying load resistance R shown in Fig. 6(a). Besides the inductor resistances listed in Table 1, the other parasitics of the converter are:

$$\begin{gathered} R_{DS_1} = 0.02\ \Omega,\ V_{D_1} = 0.6\ V,\ R_{D_1} = 0.3\Omega \\ R_{DS_2} = 0.04\ \Omega,\ V_{D_2} = 0.5\ V,\ R_{D_2} = 0.35\Omega \\ R_C = 0.2\Omega \end{gathered} \tag{38}$$

where the unknown parameters $R_{DS_i}, R_{D_i}, V_{D_i}, i = 1, 2$ and R_C represent the MOSFET on-resistance, the diode forward resistance, the conducting voltage of the diode and the capacitor equivalent series resistance, respectively of the two parallel-connected boost converter stages. Figure 6 depicts the time-varying load resistance, the contaminated output voltage $v_{cn}(t)$ used for the measurements and the output voltage $v_c(t)$. Figure 7 depicts the switching surface σ, the duty ratio u and the disturbance d and its estimate $\hat{d}$. As seen, the output response tracks the reference voltage with zero steady-state error and rejects much of the high-frequency noise due to the design of the estimator and the choice of its gains.The estimator also behaves like a continuous low-pass filter that ignores the fast switching ripples and noise of the lumped disturbance d and tracks the true average DC baseline of the estimated disturbance which in this case is $\hat{d} = -9.9694 \times 10^9$ as seen in Fig. 7(c). As these simulations show, the proposed controller is robust to noise, parameter uncertainties, parasitics and time-varying external disturbances.

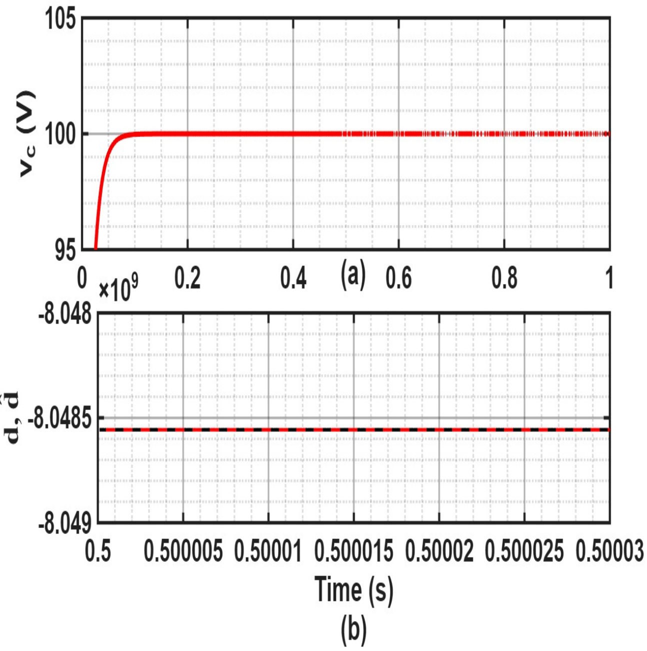

Fig. 2. Case 1: (a) Output voltage. (b) Zoomed depiction of the disturbance d in black and its estimate $\hat{d}$ in red using the averaged model and uncertain parameters listed in Table 1.

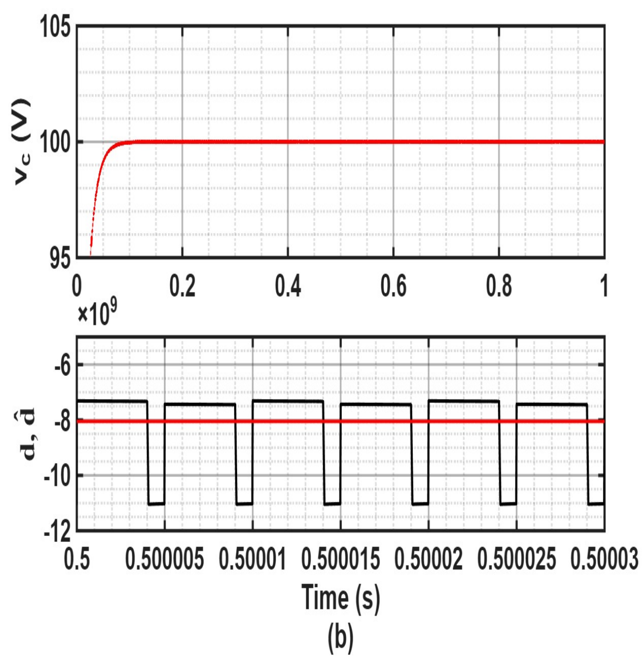

Fig. 3. Case 1: (a) Output voltage. (b) Zoomed depiction of the disturbance d in black and its estimate $\hat{d}$ in red using the switched model and the uncertain parameters listed in Table 1.

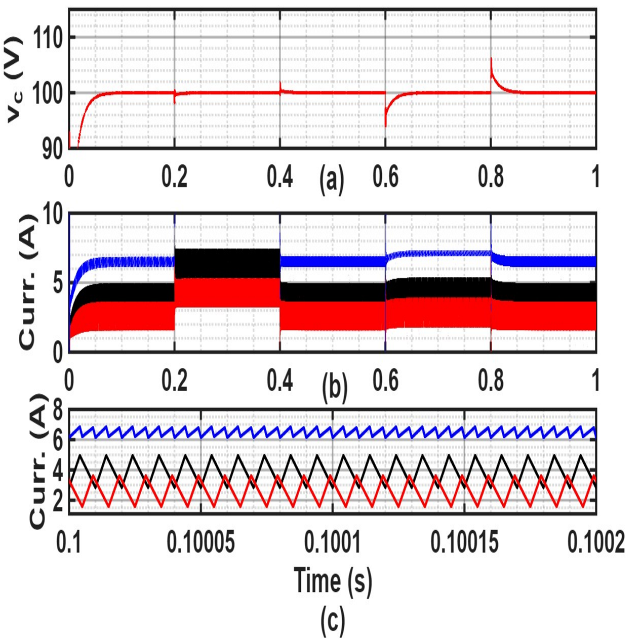

Fig. 4. Case 2: (a) output voltage response. (b) Line current i_L in blue, phase currents i_{L_1} in black and i_{L_2} in red. (c) zoomed depiction of the line and phase currents.

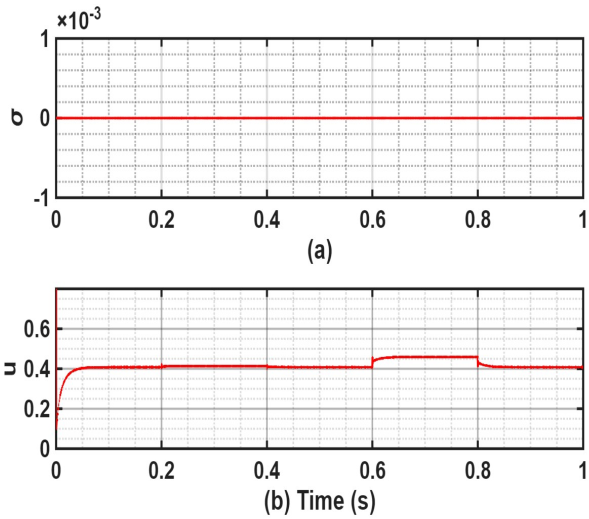

Fig. 5. Case 2: (a) sliding surface σ. (b) Duty ratio u.

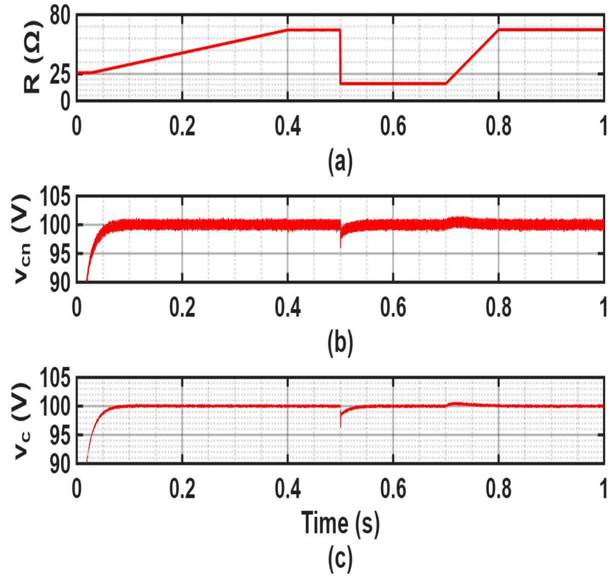

Fig. 6. Case 3: (a) Output voltage $v_c(t)$. (b) Noise contaminated measured output voltage $v_{cn}(t)$. (c) Actual output voltage $v_c(t)$.

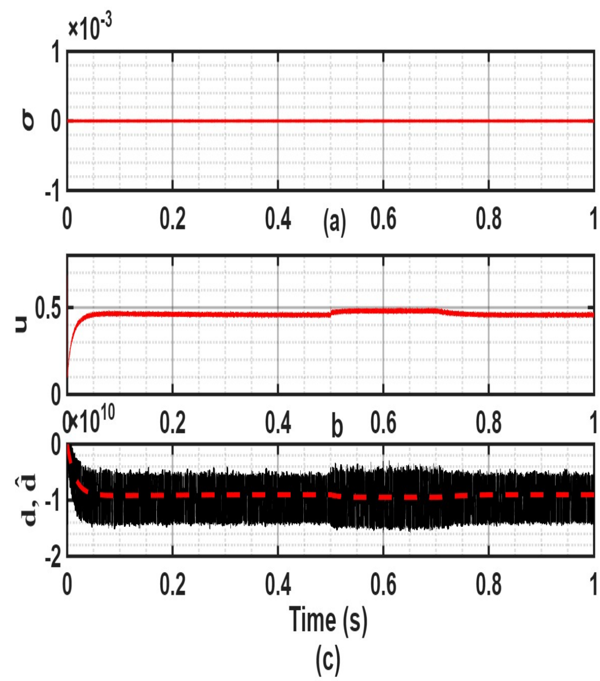

Fig. 7. Case 3: (a) Switching surface σ. (b) Duty ratio u. (c) Disturbance d in black and its estimate $\hat{d}$ in red.

IV. Conclusion

This paper presents a PWM-based, current-sensorless robust sliding mode controller for the interleaved DC-DC boost converter, requiring only a single sensor for output voltage measurement. An extended state observer successfully estimates the derivative of the output voltage along with a lumped uncertainty signal that accounts for changing load resistances and input voltages, parametric variations, and circuit parasitics. A linear sliding surface is used to derive the control law. The proposed controller has a straightforward structure and a systematic parameter-tuning procedure. Simulation results validate that the system achieves excellent disturbance suppression and dynamic compensation capabilities despite the complete absence of inductor current feedback. Future work will focus on the experimental validation of these theoretical and simulation results.

Conflict of Interest

The authors declare that there is no competing financial interest that could have appeared to influence the work reported in this paper.

References

[1] G. Cimini, G. Ippoliti, G. Orlando, S. Longhi, and R. Miceli, ”A unified observer for robust sensorless control of DC-DC converters,” Control Eng. Pract., vol. 61, pp. 21-27, Apr. 2017, doi: 10.1016/j.conengprac.2017.01.012.

[2] S. K. Pandey, S. L. Patil, U. M. Chaskar, and S. B. Phadke, ”State and disturbance observer-based integral sliding mode controlled boost DC-DC converters,” IEEE Trans. Circuits Syst. II, Exp. Briefs, vol. 66, no. 9, pp. 1567-1571, Sept. 2019, doi: 10.1109/TCSII.2018.2888570.

[3] M. Malekzadeh, A. Khosravi, and M. Tavan, ”A novel sensorless control scheme for DC-DC boost converter with global exponential stability,” Eur. Phys. J. Plus, vol. 134, no. 7, Art. no. 358, 2019, doi: 10.1140/epjp/i2019-12664-4.

[4] M. Malekzadeh, A. Khosravi, and M. Tavan, ”A novel adaptive output feedback control for DC-DC boost converter using immersion and invariance observer,” Evol. Syst., vol. 11, no. 4, pp. 707-715, 2020, doi: 10.1007/s12530-019-09268-7.

[5] X. Zhang, M. Martinez-Lopez, W. He, Y. Shang, C. Jiang, and J. Moreno-Valenzuela, ”Sensorless control for DC-DC boost converter via generalized parameter estimation-based observer,” Appl. Sci., vol. 11, no. 16, Art. no. 7761, 2021, doi: 10.3940/2076-3417/11/16/7761.

[6] S.-K. Kim and K.-B. Lee, ”Current-sensorless energy-shaping output voltage-tracking control for DC-DC boost converters with damping adaptation mechanism,” IEEE Trans. Power Electron., vol. 37, no. 8, pp. 9266-9274, Aug. 2022, doi: 10.1109/TPEL.2022.3159793.

[7] S.-K. Kim, C. Xu, and C. K. Ahn, ”Second-order disturbance-observer-based output-feedback voltage control of DC/DC converters using pole-zero cancellation,” IEEE Trans. Ind. Electron., vol. 73, no. 9, pp. 12905-12917, 2026, doi: 10.1109/TIE.2026.3677705.

[8] S. Oucheriah and A. Azad, ”Current-sensorless robust sliding mode control for the DC-DC boost converter,” AIMS Electron. Electr. Eng., vol. 9, no. 1, pp. 46-59, 2025, doi: 10.3934/electreng.2025003.

[9] W. Jiang, X. Zhang, F. Guo, J. Chen, P. Wang, and L. H. Koh, ”Large-signal stability of interleave boost converter system with constant power load using sliding-mode control,” IEEE Trans. Ind. Electron., vol. 67, no. 11, pp. 9450-9459, Nov. 2020, doi: 10.1109/TIE.2019.2955401.

[10] S. Zhuo et al., ”Robust adaptive control of interleaved boost converter for fuel cell application,” IEEE Trans. Ind. Appl., vol. 57, no. 6, pp. 6603-6610, Nov./Dec. 2021, doi: 10.1109/TIA.2021.3113262.

[11] H. Sartipizadeh, F. Harirchi, M. Babakmehr, and P. Dehghanian, ”Robust model predictive control of DC-DC floating interleaved boost converter with multiple uncertainties,” IEEE Trans. Energy Convers., vol. 36, no. 2, pp. 1403-1412, June 2021, doi: 10.1109/TEC.2021.3058524.

[12] J. Wachter, L. Grll, and V. Hagenmeyer, ”Experimental analysis of immersion and invariance adaptive control for an interleaved DC/DC boost converter with unknown load type,” in Proc. IEEE PES Innov. Smart Grid Technol. Eur. (ISGT EUROPE), Grenoble, France, 2023, pp. 1-6, doi: 10.1109/ISGTEUROPE56780.2023.10407194.

[13] Z. Dai, J. Liu, K. Li, Z. Mai, and G. Xue, ”Research on a modeling and control strategy for interleaved boost converters with coupled inductors,” Energies, vol. 16, no. 9, Art. no. 3810, 2023, doi: 10.3390/en16093810.

[14] A. Sferlazza et al., ”Robust disturbance rejection control of DC/DC interleaved boost converters with additional sliding mode component,” in Proc. Asia Meet. Environ. Electr. Eng. (EEE-AM), Hanoi, Vietnam, 2023, pp. 1-6, doi: 10.1109/EEEAM58328.2023.10395325.

[15] S. V. Malge et al., ”Inductor current estimation based sensorless control of boost type DC-DC converter,” Control Eng. Pract., vol. 153, Art. no. 106119, 2024, doi: 10.1016/j.conengprac.2024.106119.

[16] A. Mishra et al., ”Non-linear control of interleaved boost converter using disturbance observer-based approach,” IEEE Access, vol. 13, pp. 23833-23840, 2025, doi: 10.1109/ACCESS.2025.3537826.

[17] G. Garraffa et al., ”Robust control of interleaved boost converter with active disturbance compensation,” Control Eng. Pract., vol. 169, Art. no. 106746, 2026, doi: 10.1016/j.conengprac.2025.106746.